Chinese Chemical Letters 31 (2020) 1014–1017

Contents lists available at ScienceDirect

Chinese Chemical Letters

journal homepage: www.elsevier.com/locate/cclet

Communication

Robust and easily retrievable Pd/$Ti_3C_2T_x$⊂graphene hydrogels for efficient catalytic hydrogenation of nitroaromatic compounds

Xiuqiang Xie[a,*], Zhenjun Wu[b], Nan Zhang[a,*]

[a] College of Materials Science and Engineering, Hunan University, Changsha 410082, China
[b] College of Chemistry and Chemical Engineering, Hunan University, Changsha 410082, China

ARTICLE INFO

Article history:
Received 14 September 2019
Received in revised form 10 October 2019
Accepted 12 October 2019
Available online 22 October 2019

Keywords:
$Ti_3C_2T_x$
Hydrogels
Robust structure
Convenient recyclability
Nitroaromatic compounds hydrogenation

ABSTRACT

$Ti_3C_2T_x$ has been emerging as an attractive platform to prepare composite catalysts, and their assembly into integrated catalytic materials represents a key step forward toward practical applications. However, the swelling behavior of $Ti_3C_2T_x$ leads to significant structure change, which challenges the stability of $Ti_3C_2T_x$-based integrated functional materials for catalytic applications. Here we report a facile synthesis of Pd/$Ti_3C_2T_x$⊂graphene hydrogels in which Pd/$Ti_3C_2T_x$ are spatially encapsulated in the 3D porous graphene framework. The porous interconnected structure not only affords efficient mass transfer and desirable functional accessibility to catalytic active sites, but also effectively buffers the swelling behavior of $Ti_3C_2T_x$. When applied for catalytic hydrogenation of nitroaromatic compounds, the mechanically robust Pd/$Ti_3C_2T_x$⊂graphene hydrogels exhibit efficient activities, easy separability, and good cyclability. This work is expected to promote the application of $Ti_3C_2T_x$-based functional materials for practical applications involving interactions with salt solutions, such as supercapacitors, catalysis, and water purification.

MXenes are a family of two-dimensional (2D) layered transition metal carbides/nitrides, which are composed of hexagonal $M_{n+1}X_nT_x$ structures, where M is a transition metal, X is C and/or N, T_x stands for the functional terminations (such as -O-, −OH and -F), and n = 1, 2 or 3 [1–4]. As a typical member in MXene family, $Ti_3C_2T_x$ features several advantages, including high conductivity associated with high electron density of states near Fermi level, excellent hydrophily, and rich surface chemistry [5]. The tunability of their physicochemical properties renders $Ti_3C_2T_x$ very promising for hybridization with nanomaterials and the interest in $Ti_3C_2T_x$–based functional materials has been largely increasing recently [6–18]. Computational investigations demonstrated that Ti_3C_2 has stronger interactions with noble metals (NMs) than graphene counterpart, the forebear of 2D materials [19]. Especially, the adsorption energy is −4.68 eV for Pd@Ti_3C_2, which is higher than that of Pd@graphene (−1.08 eV). Similar observations have also been found for Au, Pt and Ru [19]. The strong metal-support interactions (SMSI) lead to large electronic perturbations in the supported NMs, which are suggested to modulate the metal *d*-band center, thus often leading to significantly enhanced catalytic activities as a result [20–23]. NMs/$Ti_3C_2T_x$ composite functional materials have shown promising performances for catalytic hydrogenation of nitro compounds [24], electrocatalytic and photocatalytic hydrogen evolution [25–27]. However, the reported NMs/$Ti_3C_2T_x$ composites are powder catalysts in most cases, which require time-consuming recycling processes after catalytic reactions. In this context, it is desirable to develop easily retrievable NMs/$Ti_3C_2T_x$ catalysts with high catalytic activities.

Integrated catalytic materials are attractive as they are conveniently retrievable for practical applications. In this realm, film materials and monoliths are the typical representatives [28,29]. Notably, the integrated functional materials should be able to maintain structure integrity while exhibiting high catalytic performances. However, the swelling of $Ti_3C_2T_x$ due to the superior hydrophilic nature of surface functional groups and salts penetration can lead to the weakening of the adhesion forces between $Ti_3C_2T_x$ and substrates [30], which destroys the integrity of $Ti_3C_2T_x$–based films upon prolonged reaction time. This issue significantly challenges the recyclability of $Ti_3C_2T_x$–based film catalysts. Alternatively, monolithic hydrogels are not only easily retrievable, but also characteristic of hierarchical porous structures to substantially inhibit the aggregation of subunits, thus exposing

* Corresponding authors.
E-mail addresses: xiuqiang_xie@hnu.edu.cn (X. Xie), nanzhang@hnu.edu.cn (N. Zhang).

https://doi.org/10.1016/j.cclet.2019.10.012

more accessible surface-active sites [31]. In addition, the interconnected porous structure could buffer the swelling behavior of $Ti_3C_2T_x$ during catalytic reactions. Consequently, NMs/$Ti_3C_2T_x$-based hydrogels hold great promises as robust and easily retrievable monolithic functional materials for catalytic applications. However, the research in this regard is still lacking.

Herein, we report the preparation of Pd/$Ti_3C_2T_x$ encapsulated in 3D graphene networks, *i.e.*, Pd/$Ti_3C_2T_x$⊂graphene hydrogels, and the application for the catalytic hydrogenation of nitroaromatic compounds, which is an important chemical transformation for organic synthesis and industrial production [32]. It is demonstrated that Pd/$Ti_3C_2T_x$⊂graphene hydrogels exhibit good catalytic performances for the hydrogenation of nitroaromatic compounds and are easily retrievable without structure damage, which is promising for practical applications.

Fig. 1a shows the schematics for the preparation of Pd/$Ti_3C_2T_x$⊂graphene hydrogels by a two-step process. By utilizing the redox capability of $Ti_3C_2T_x$, Pd nanoparticles have been firstly deposited on $Ti_3C_2T_x$ by an *in-situ* reduction process based on a simple redox reaction between $PdCl_4^{2-}$ and $Ti_3C_2T_x$ in an aqueous solution [5]. Taking advantage of the cross-linking phenomenon during the reduction of graphene oxide (GO) to graphene and the interaction between graphene and $Ti_3C_2T_x$ [29], Pd/$Ti_3C_2T_x$ was subsequently encapsulated in graphene hydrogel by a GO-assisted assembly process, which generates Pd/$Ti_3C_2T_x$⊂graphene composite hydrogels as a result. Fig. 1b shows the X-ray diffraction (XRD) pattern of the resulting Pd/$Ti_3C_2T_x$⊂graphene. Similar to pure $Ti_3C_2T_x$ (Fig. S1a in Supporting information), a diffraction peak at around 5.4° can be seen, which is ascribed to the (0002) crystal plane of $Ti_3C_2T_x$ with an interlayer distance of 1.6 nm. In addition, the diffraction peaks corresponding to metallic Pd are clearly observed, which is in agreement with the XRD results of Pd/$Ti_3C_2T_x$ composites (Fig. S1b in Supporting information), evidencing the presence of Pd. We further investigated the composition of the resulting hydrogel by Raman spectrum. As shown in Fig. 1c, the mode at 198 cm^{-1} is A_{1g} symmetric out-of-plane vibration, while the modes at 377 cm^{-1} and 626 cm^{-1} are the E_g group vibrations of $Ti_3C_2T_x$. In addition, two Raman peaks located at 1328 cm^{-1} and 1547 cm^{-1} are present, which are ascribed to the D band and G band of graphene, respectively. The Raman result suggests the successful hybridization between $Ti_3C_2T_x$ and graphene in the as-prepared hydrogel.

The microstructures of the resulting Pd/$Ti_3C_2T_x$⊂graphene hydrogel have been investigated by scanning electron microscopy (SEM) and transmission electron microscopy (TEM). As can be seen from the SEM image in Fig. 2a, Pd/$Ti_3C_2T_x$⊂graphene exhibits a well-defined 3D interconnected network with hierarchical macropores in the range of several micrometers. Moreover, abundant nanoparticles are found to accommodate on the surface of the backbone, which are reasonably speculated to be Pd. The porous channels could facilitate mass transfer of reactants, while the deposition of Pd nanoparticles on the 3D network benefits the exposure of active sites to reactants, which are desirable for catalytic applications, as discussed later. Fig. 2b displays the TEM image of the as-synthesized Pd/$Ti_3C_2T_x$⊂graphene. The typical flake-like morphology can be clearly seen and the surface is decorated with Pd nanoparticles. The inset in Fig. 2b is the corresponding selected-area electron diffraction (SAED) pattern with diffraction rings indexed to the (111) and (200) planes of the cubic Pd, respectively. The high-resolution TEM (HRTEM) image shown in Fig. 2c displays clear lattice fringes, the spacing of which is measured to be *ca.* 0.23 nm, corresponding to the (111) crystal plane of cubic Pd (Fig. 2d). On the other hand, an interlayer spacing of 1.6 nm indexed to the (0002) plane of $Ti_3C_2T_x$ is also observed, which coincides with the result from XRD analysis. The particle size of Pd has also been statistically analyzed, based on which the average size of Pd particles is 14.3 nm (Fig. 2e). Fig. S2 (Supporting information) shows the N_2 adsorption–desorption isotherm of the resulting 3D Pd/$Ti_3C_2T_x$⊂graphene. The Brunauer–Emmett–Teller (BET) surface area of the Pd/$Ti_3C_2T_x$⊂graphene hydrogel is measured to be 51 m^2/g.

To evaluate the catalytic activities of the as-prepared Pd/$Ti_3C_2T_x$⊂graphene hydrogel, the selective hydrogenation of 4-nitroaniline (4-NA) to *p*-phenylenediamine (PPD) is chosen as a model reaction. It is well-known that PPD is an important organic intermediate widely used in the production of different types of products such as dyes, rubber antioxidants and aramid textile fibers [33,34]. As shown in Fig. S3 (Supporting information), in the presence of Pd/$Ti_3C_2T_x$⊂graphene hydrogel, the absorption peak of 4-NA is rapidly decreased and two peaks at 238 and 305 nm simultaneously appeared. These two peaks can be attributed to the characteristic peaks of PPD [34], indicating the successful transformation of 4-NA to PPD by the Pd/$Ti_3C_2T_x$⊂graphene monolithic catalyst. The hydrogenation reaction proceeds very fast over Pd/$Ti_3C_2T_x$⊂graphene (Fig. 3a). After 1 min, 91% of 4-NA

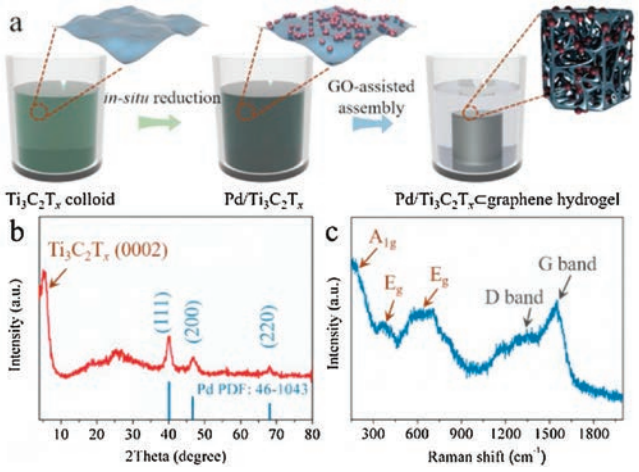

Fig. 1. (a) Schematic illustration for the preparation of Pd/$Ti_3C_2T_x$⊂graphene hydrogels. (b) XRD pattern and (c) Raman spectrum of Pd/$Ti_3C_2T_x$⊂graphene hydrogels.

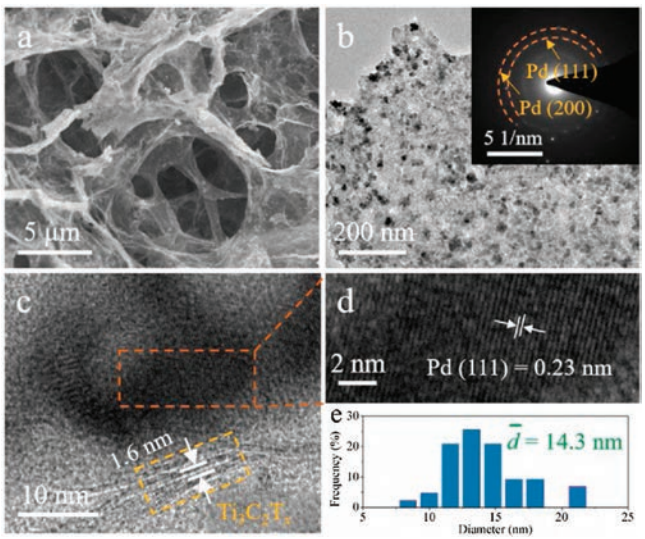

Fig. 2. (a) SEM image of Pd/$Ti_3C_2T_x$⊂graphene hydrogels. (b) TEM image of Pd/$Ti_3C_2T_x$⊂graphene. The inset shows the SAED pattern. (c, d) TEM image of Pd/$Ti_3C_2T_x$⊂graphene. (e) Size distribution of Pd nanoparticles in the Pd/$Ti_3C_2T_x$⊂graphene hydrogel.

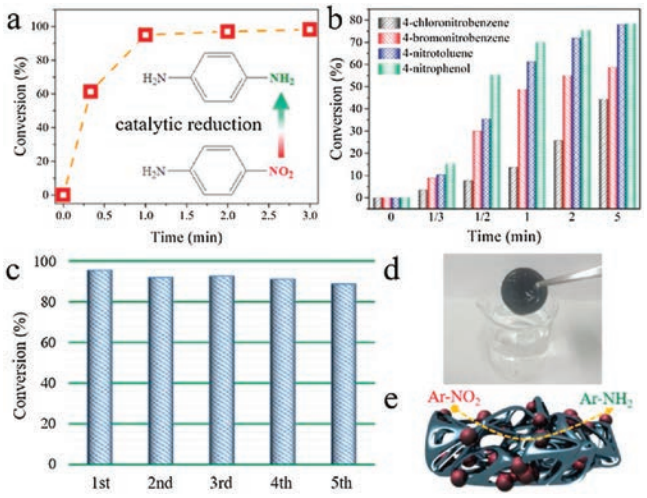

Fig. 3. Catalytic performance of the Pd/$Ti_3C_2T_x$⊂graphene hydrogel for the hydrogenation of (a) 4-NA, and (b) other nitroaromatic compounds with different substituents. (c) Photo of the Pd/$Ti_3C_2T_x$⊂graphene hydrogel after the catalytic hydrogenation of 4-NA. (d) Cycling performance of the Pd/$Ti_3C_2T_x$⊂graphene hydrogel for the hydrogenation of 4-NA. (e) Schematics of catalytic hydrogenation of nitroaromatic compounds over Pd/$Ti_3C_2T_x$⊂graphene hydrogels.

has been converted. For comparison, Pd/$Ti_3C_2T_x$ films deposited on the substrate of poly(vinylidene fluoride) (PVDF) have also been prepared (Fig. S4 in Supporting information). In comparison, only 62.9% of 4-NA has been converted over Pd/$Ti_3C_2T_x$ (Fig. S5 in Supporting information). These results demonstrate the structure superiority of the 3D porous Pd/$Ti_3C_2T_x$⊂graphene hydrogel, which is favorable for the accessibility of active sites for catalytic applications. In addition, we have investigated the activities of the Pd/$Ti_3C_2T_x$⊂graphene hydrogel towards the hydrogenation of other nitroaromatic compounds with different substituent groups. The results in Fig. 3b show that, for these different nitroaromatic compounds, the Pd/$Ti_3C_2T_x$⊂graphene catalyst also exhibits high catalytic performance. The conversions of the substrates are closely related to the electron withdrawing or electron donating nature of the substituents in the aromatic rings. It is found that Pd/$Ti_3C_2T_x$⊂graphene exhibits higher activity for the substrates with electron donating groups, such as $-CH_3$ and $-OH$, than that with electron withdrawing substituents, such as –Cl and –Br, under the same conditions, which is in agreement with previous reports [35]. Furthermore, as the electron donating capacity of $-OH$ is higher than that of $-CH_3$, the reaction rate for nitrophenol is higher than that of nitrotoluene [35].

Then the stability of the Pd/$Ti_3C_2T_x$⊂graphene hydrogel toward catalytic hydrogenation of 4-NA has been examined by the successive recycle tests. As displayed in Fig. 3c, during the five times recycle test, Pd/$Ti_3C_2T_x$⊂graphene hydrogel exhibits stable performance. Besides, the as-prepared Pd/$Ti_3C_2T_x$⊂graphene hydrogel successfully maintains the structure stability and is easily separated from the reaction system by using a tweezer (Fig. 3d), which suggests the robust mechanical property and is desirable for practical applications. In contrast, the Pd/$Ti_3C_2T_x$ film became fragile and peeled off from the PVDF substrate during the catalytic process (Fig. S6a in Supporting information). Meanwhile, many small Pd/$Ti_3C_2T_x$ pieces were found in the reaction medium (Fig. S6b in Supporting information). Considering that $Ti_3C_2T_x$ surfaces are hydrophilic due to the terminations of –O–, $-OH$ and –F, of particular interest is H_2O sorption/intercalation, which could lead to significant structural change of $Ti_3C_2T_x$. In the present reaction system, Na^+ ions are present in the aqueous solution, which intercalate into $Ti_3C_2T_x$ layers spontaneously [36]. When these cations intercalate the structure, they often carry interlayer solvating water (H_2O) molecules. In other words, the presence of Na^+ between $Ti_3C_2T_x$ layers is accompanied by the intercalation of a bilayer of H_2O molecules due to the cation solvation reactions, as revealed by Ghidiu *et al.*, which result in the swelling behavior [37]. The swelling behavior leads to the volume expansion of Pd/$Ti_3C_2T_x$ films, thus weakening the adhesion forces between $Ti_3C_2T_x$ and the substrate, as well as intersheet interactions. As a result, the integrity of Pd/$Ti_3C_2T_x$ films has been destroyed during catalytic processes. In sharp contrast, the porous and 3D interconnected structure is able to buffer the swelling behavior of $Ti_3C_2T_x$ to maintain the structure stability during catalytic processes, as schematically depicted in Fig. 3e. Such effect thus affords mechanically robust and easily retrievable Pd/$Ti_3C_2T_x$⊂graphene hydrogels as the integrated catalysts. Meanwhile, the porous structure of the as-prepared Pd/$Ti_3C_2T_x$⊂graphene hydrogels is beneficial for mass transfer of reactants and maximizes the functional accessibility of the catalyst of Pd nanoparticles, which is of key importance for achieving efficient catalytic performances. These result further highlights the structural advantage of the Pd/$Ti_3C_2T_x$⊂graphene hydrogel for catalytic applications.

In summary, Pd/$Ti_3C_2T_x$⊂graphene hydrogels with 3D interconnected porous structure have been successfully prepared by a facile two-step process. The as-prepared Pd/$Ti_3C_2T_x$⊂graphene hydrogels display efficient catalytic activities for the hydrogenation of various nitroaromatic compounds. In addition, a comparison between Pd/$Ti_3C_2T_x$⊂graphene hydrogels and Pd/$Ti_3C_2T_x$ films as typical integrated catalysts reveals the prominent structure advantage of the porous hydrogel over the film in buffering the swelling behavior of $Ti_3C_2T_x$ during catalytic processes. This renders Pd/$Ti_3C_2T_x$⊂graphene hydrogels the mechanically robust, easily retrievable, and cycling-stable catalysts for continuous catalytic applications.

Declaration of competing interest

The authors declare no competing financial interests.

Acknowledgments

The support from the National Natural Science Foundation of China (Nos. 51802040, 51977071 and 21802020), Key Laboratory of Coal to Ethylene Glycol and Its Related Technology, Chinese Academy of Sciences (No. 201901), and Natural Science Foundation of Hunan Prvoince (No. 2017JJ2040) is gratefully acknowledged. N. Zhang and X. Xie also acknowledge the Fundamental Research Funds for the Central Universities.

Appendix A. Supplementary data

Supplementary material related to this article can be found, in the online version, at doi:https://doi.org/10.1016/j.cclet.2019.10.012.

References

[1] M. Naguib, M. Kurtoglu, V. Presser, et al., Adv. Mater. 23 (2011) 4248–4253.
[2] B. Anasori, M.R. Lukatskaya, Y. Gogotsi, Nat. Rev. Mater. 2 (2017) 16098.
[3] H. He, Q. Xia, B. Wang, et al., Chin. Chem. Lett. 31 (2020) 984–987.
[4] M. Li, J. Lu, K. Luo, et al., J. Am. Chem. Soc. 141 (2019) 4730–4737.
[5] E. Satheeshkumar, T. Makaryan, A. Melikyan, et al., Sci. Rep. 6 (2016) 32049.
[6] X. Xie, C. Chen, N. Zhang, et al., Nature Sustain. 2 (2019) 856–862.
[7] J. Luo, W. Zhang, H. Yuan, et al., ACS Nano 11 (2017) 2459–2469.
[8] J. Yan, C.E. Ren, K. Maleski, et al., Adv. Funct. Mater. 27 (2017) 1701264.
[9] M.Q. Zhao, X. Xie, C.E. Ren, et al., Adv. Mater. 29 (2017) 1702410.
[10] X. Tang, X. Guo, W. Wu, G. Wang, Adv. Energy Mater. 8 (2018) 1801897.
[11] Y.T. Liu, P. Zhang, N. Sun, et al., Adv. Mater. 30 (2018) 1707334.
[12] Y. Dong, S. Zheng, J. Qin, et al., ACS Nano 12 (2018) 2381–2388.
[13] Y. Fang, B. Yang, D. He, et al., Chin. Chem. Lett. 31 (2020) 1004–1008.

[14] L. Ding, Y. Wei, L. Li, et al., Nat. Commun. 9 (2018) 155.
[15] C. Zhang, S.-H. Park, A. Seral-Ascaso, et al., Nat. Commun. 10 (2019) 849.
[16] H. Liu, X. Zhang, Y. Zhu, et al., Nano-Micro Lett. 11 (2019) 65.
[17] X. Zhang, Y. Guo, Y. Li, Y. Liu, S. Dong, Chin. Chem. Lett. 30 (2019) 502–504.
[18] Q. Zhao, Q. Zhu, J. Miao, P. Zhang, B. Xu, Nanoscale 11 (2019) 8442–8448.
[19] Y. Gao, Y. Cao, Y. Gu, et al., Appl. Surf. Sci. 465 (2019) 911–918.
[20] S.J. Tauster, S.C. Fung, R.L. Garten, J. Am. Chem. Soc. 100 (1978) 170–175.
[21] C.T. Campbell, Nat. Chem. 4 (2012) 597.
[22] N. Acerbi, S.C.E. Tsang, G. Jones, S. Golunski, P. Collier, Angew. Chem. Int. Ed. 52 (2013) 7737–7741.
[23] B.D. Chandler, Nat. Chem. 9 (2017) 108.
[24] K. Li, T. Jiao, R. Xing, et al., Green Energy Environ. 3 (2018) 147–155.
[25] Z. Li, Z. Qi, S. Wang, et al., Nano Lett. 19 (2019) 5102–5108.
[26] S. Min, Y. Xue, F. Wang, Z. Zhang, H. Zhu, Chem. Commun. 55 (2019) 10631–10634.
[27] C. Cui, R. Cheng, C. Zhang, X. Wang, Chin. Chem. Lett. 31 (2020) 988–991.
[28] X. Zhang, Z. Su, Adv. Mater. 24 (2012) 4574–4577.
[29] Y. Chen, X. Xie, X. Xin, Z.R. Tang, Y.J. Xu, ACS Nano 13 (2019) 295–304.
[30] C.E. Ren, M. Alhabeb, B.W. Byles, et al., ACS Appl. Nano Mater. 1 (2018) 3644–3652.
[31] X. Xie, N. Zhang, Z.R. Tang, Y.J. Xu, Chem. Sci. 9 (2018) 8876–8882.
[32] N. Zhang, S. Xie, B. Weng, Y.J. Xu, J. Mater. Chem. A 4 (2016) 18804–18814.
[33] W. Wu, G. Liu, Q. Xie, et al., Green Chem. 14 (2012) 1705–1709.
[34] X. Xie, N. Zhang, Z.R. Tang, M. Anpo, Y.J. Xu, Appl. Catal. B: Environ. 237 (2018) 43–49.
[35] P. Deka, R. Choudhury, R.C. Deka, P. Bharali, RSC Adv. 6 (2016) 71517–71528.
[36] M.R. Lukatskaya, O. Mashtalir, C.E. Ren, et al., Science 341 (2013) 1502.
[37] M. Ghidiu, J. Halim, S. Kota, et al., Chem. Mater. 28 (2016) 3507–3514.